ISBN: 978-3-95450-253-0 ISSN: 2673-5571 doi:10.18429/JACoW-HB2023-WEC2C1

EVALUATION OF POWER DEPOSITION IN HL-LHC WITH CRYSTAL-ASSISTED HEAVY ION COLLIMATION*

V. Rodin†, R. Bruce, R. Cai, M. D'Andrea, L. S. Esposito, A. Lechner,

J.-B. Potoine, S. Redaelli, P. Schoofs, CERN, Geneva, Switzerland

Abstract

The LHC heavy-ion program, utilizing $^{208}Pb^{82+}$ beams with an energy of up to 7 ZTeV, will profit from significantly higher beam intensities in future runs. During periods of short beam lifetime, a potential performance limitation may arise from secondary ions produced through electromagnetic dissociation and hadronic fragmentation in the collimators of the betatron cleaning insertion. These off-rigidity fragments risk quenching superconducting magnets when they are lost in the dispersion suppressor. To address this concern, an alternative collimation scheme will be introduced for forthcoming heavy ion runs, employing bent channeling crystals as primary collimators. In this contribution, we detail a thorough study of power deposition levels in superconducting magnets through multi-turn halo dynamics and FLUKA shower simulations for the crystal-based collimation system. The study focuses on the downstream dispersion suppressor regions of the betatron cleaning insertion, where the quench risk is the highest. Based on this work, we quantify the expected quench margin in future runs with $^{208}Pb^{82+}$ beams, providing crucial insights for the successful execution of the upgraded heavy-ion program at the HL-LHC.

INTRODUCTION

In 2023, the LHC heavy-ion program will profit for the first time from High Luminosity LHC (HL-LHC) beam intensities [1]. Numerous improvements were carried out within the LIU [2] and HL-LHC projects [3], which allow for beam intensities above 2×10^{11} $^{208}Pb^{82+}$ ions. Moreover, the $^{208}Pb^{82+}$ energy will be increased from the previous operational value of 6.37 ZTeV in 2018 to 6.8 ZTeV in 2023, with a total stored beam energy expected to reach about 20 MJ. In a superconducting machine like the LHC, even a small fraction of such stored energy is enough to cause quenches of superconducting magnets [3–5]. To counter the adverse effects of beam halo losses, multi-stage betatron and momentum collimation systems are installed in the LHC [6]. In conjunction with the Beam Loss Monitor (BLM) system [7], which continuously monitors beam losses and can trigger beam aborts, this setup protects from beam-induced quenches and, in the worst case, against potential damage to the accelerator equipment.

The collimation of heavy-ion beams poses a greater challenge compared to regular LHC proton operation, due to the occurrence of nuclear fragmentation and electromagnetic dissociation (EMD) when particles interact with the collimator material. These processes enhance particle leakage to cold magnets and hence the likelihood of beam-induced quenches. In order to improve the collimation efficiency for ions, crystal-assisted halo collimation [8, 9] has been implemented for $^{208}Pb^{82+}$ operation as part of the HL-LHC baseline [3]. The system will be used for the first time with high beam intensities in the 2023 heavy-ion run [10, 11]. Bent crystals can be used to guide halo particles onto a secondary collimator, limiting nuclear and electromagnetic fragmentation in the primary beam-intercepting device thanks to the channeling process. Fragments produced in the secondary collimator are much less likely to reach cold magnets, which increases the maximum allowed beam power loss without quenching.

Given the first operational use of crystal collimation in 2023, it is essential to assess the expected quench margin for the 2023 machine configuration (6.8 ZTeV) by predicting the power deposition in superconducting dispersion suppressor (DS) magnets next to the betatron cleaning insertion. A beam-induced quench in case of a significant beam lifetime drop would impose a machine downtime of eight or more hours, during which the affected superconducting magnets need to be brought back to their operational temperature. Quenches can be prevented by triggering a BLM abort when a certain loss threshold is exceeded. However, if thresholds are set too conservatively, this can lead to premature beam dumps, which would affect the machine availability. An accurate understanding of the expected power deposition in cold magnets is therefore crucial for setting BLM abort thresholds and for optimizing the performance. This paper presents the results of FLUKA [12–14] simulations that quantify the amount of power deposited in magnet coils for Run 3 operational conditions. It also provides an overview of crystal-assisted heavy ion collimation in the LHC, together with a brief introduction to the channeling process.

CRYSTAL-ASSISTED COLLIMATION

The multi-stage collimation system of the LHC was designed and put in place before launching operation in 2008 [3]. It contains two main sub-systems located in different insertion regions (IRs), the betatron cleaning system in IR7 and the off-momentum cleaning system in IR3. Currently, the collimation system comprises a total of more than 100 collimators for both beams. The betatron halo cleaning in IR7 is done with a three-stage collimator hierarchy for protons, with the addition of bent silicon crystals for ions, which substitute the standard primary collimators in

* Research supported by the HL-LHC project.
† volodymyr.rodin@cern.ch

ISBN: 978-3-95450-253-0 ISSN: 2673-5571 doi:10.18429/JACoW-HB2023-WEC2C1

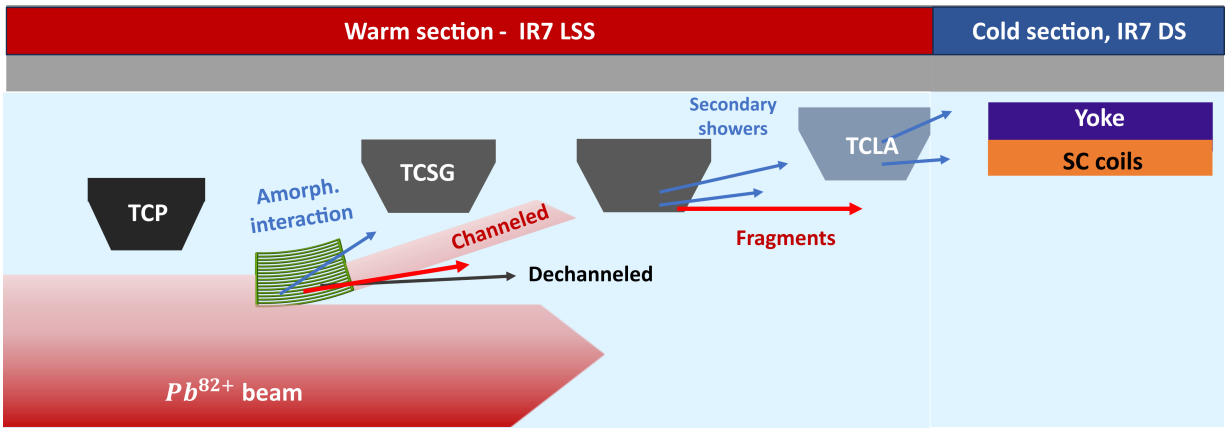

Figure 1: Collimation hierarchy in IR7 for heavy-ion operation. The bent crystal is the closest element to the ion beam orbit.

future $^{208}Pb^{82+}$ runs. A schematic layout of the collimation hierarchy in IR7 is illustrated in Fig. 1.

When using the standard collimation system, the jaws of the primary collimators (TCPs) are the closest elements to the beam in the whole ring. Thus, they intercept halo particles at large betatron oscillation amplitudes. Secondary particle showers and ion fragments escaping from the primary collimators are intercepted by secondary collimators (called TCSGs) and further downstream by shower absorbers (TCLAs). These collimators have larger gaps, measured in terms of the beam sigma (σ) units, accommodating the circulating beam and effectively capturing secondary particles.

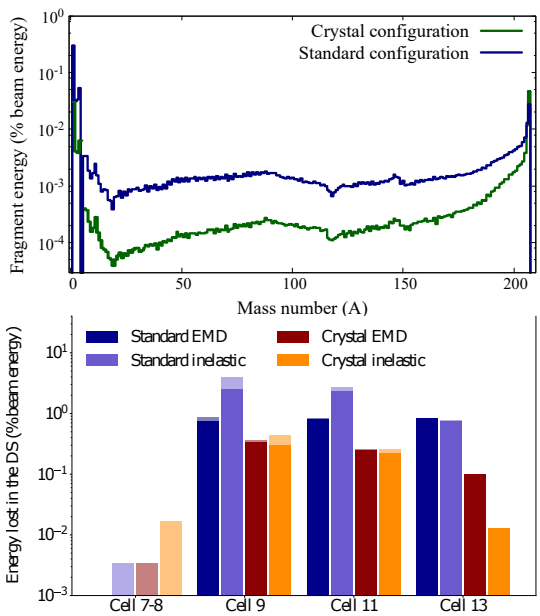

Figure 2: Top: energy fraction carried by secondary ion fragments escaping from the standard primary collimator and the crystal, respectively. Bottom: breakdown of the energy lost on the cold magnet aperture in different lattice cells of the DS and arc downstream of the betatron cleaning insertion. Darker colors correspond to the contribution of heavy fragments ($Z \geq 80$). The figures originate from Ref. [5].

The cleaning process utilises a set of collimators with a different azimuthal orientation around the beam axis (horizontal, vertical and skew), thus forming an envelope around the beam transverse shape.

In a circular machine like the LHC, beam halo particles can traverse a primary collimator multiple times before undergoing either an inelastic nuclear interaction or electromagnetic dissociation. Once the beam particles are subject to a collision, a small fraction of secondary fragments can escape from the collimation hierarchy and get lost elsewhere because of their slightly different magnetic rigidity compared to the beam particles. Notably, these secondaries can get lost on the cold aperture in the dispersion suppressor and arc downstream of IR7 due to the beam optics with peaks in the dispersion function. During heavy-ion operation, a variety of secondary ion fragments can emerge and leak to the cold region, resulting in a reduced collimation efficiency compared to proton runs. Most of the fragments lost in cold magnets emerge directly from the primary collimators.

Crystal-assisted collimation is an advanced collimation technique that can reduce the secondary fragment leakage to cold magnets. Positively charged beam particles like the fully stripped $^{208}Pb^{82+}$ ions in the LHC can be captured within the atomic planes of a crystal lattice if they enter the crystal with a momentum nearly parallel to the atomic planes (see next section for details). If a crystal is bent mechanically, it can deflect incoming heavy ions by tens of microradians, much more than typical scattering angles achieved with amorphous materials. In case of crystal-assisted collimation, the crystals are used as primary collimators (see Fig. 1), which steer channeled ions on a secondary absorber. The main advantage of such a system is the reduced number of $^{208}Pb^{82+}$ ions fragment in the primary beam-intercepting device. A detailed study of the fragment production and leakage for the crystal-assisted system was presented in Ref. [5], quantifying the expected reduction of EMD and inelastic interaction rates in the crystal when compared to the standard collimation system. The obtained fragment distributions and the resulting energy loss in different DS and arc cells are depicted in Fig. 2.

ISBN: 978-3-95450-253-0 ISSN: 2673-5571 doi:10.18429/JACoW-HB2023-WEC2C1

COHERENT PHENOMENA IN BENT CRYSTALS

The occurrence of channeling arises when positively charged particles are trapped inside the electrostatic potential between neighboring planes of the crystalline lattice. The height of the potential well U_{max} depends on the material and plane orientation and is ≈ 20 eV for the Si (110) planes orientation used in the LHC crystals. In order to be trapped within this potential, the angle θ_{in} between the particle momentum and the channel orientation should be smaller than the critical angle θ_c. This quantity depends on the velocity v and momentum p of the particle as well as the height of the potential well:

$$\theta_c = \sqrt{\frac{2U_{max}}{pv}}. \quad (1)$$

Bending the crystal by an angle θ_b distorts its inter-planar potential well symmetry. When a particle impacts the crystal at an angle $\theta_{in} > \theta_c$ and a direction that may become tangent to the crystalline planes, it encounters a potential barrier greater than its transverse energy. As a result, the particle is reflected in the direction opposite to the crystal bending by an angle $\approx 1.4 \times \theta_c$. This phenomenon is referred to as volume reflection (VR). Volume reflection efficiency exceeds that of channeling and, at LHC energies, has a larger angular acceptance, equal to the crystal bending θ_b. Volume reflection was initially considered for beam collimation due to its high efficiency. However, channeling was preferred because it reduces the rate of nuclear interactions and allows for larger deflection angles.

A channeled particle through a crystal can interact with the electrons and nuclei of the crystal lattice. Some of the interactions may increase the particle's transverse energy, causing it to exceed the potential well U_{max}. This effect is called dechanneling (DCH) and is the primary source of the reduction in channeling efficiency. Dechanneled particles are deflected by an angle smaller than θ_b.

The reverse process, known as volume capture (VC), can also occur. Particles which are not initially channeled may interact with nuclei and electrons, reducing their transverse energy and becoming trapped in the planar channeling potential. While this process occurs within the same acceptance angles as VR, it happens with a lower probability.

Additional details about other interaction modes occurring during the transition between amorphous (AM) and VR regions can be found in Refs. [15–17]. The FLUKA code is proven to be capable of accurate modeling of channeling processes [14], enabling accurate predictions of the final direction and position of heavy-ion halo particles after interaction with a crystal collimator. Figure 3 displays FLUKA simulation results of an LHC crystal's angular scan with a proton beam at the injection energy of 450 GeV, showcasing the diverse interaction modes that particles undergo while crossing the crystal.

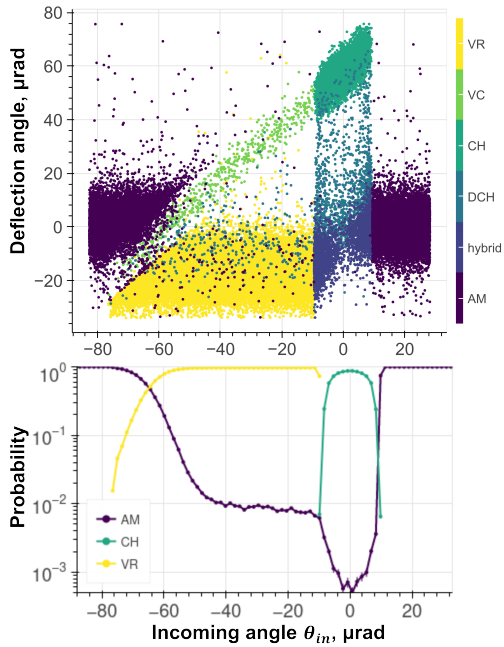

Figure 3: Top: simulation distribution of the particle deflection at the exit of a crystal with a bending angle of 50 µrad, as a function of the incoming angle. Different interaction modes are represented using distinct colors. Bottom: probability of the most relevant interaction modes in halo cleaning as a function of the incoming angle.

SIMULATION SETUP

To estimate power deposition levels inside magnet coils, collimator jaws and other equipment, a multi-step simulation chain was developed and adopted at CERN [18]. The initial step involves multi-turn tracking in SixTrack [19, 20], coupled with FLUKA to realistically model interactions with collimators and crystals [21]. More details on this part can be found in Refs. [18, 22]. The second simulation step is entirely conducted within a stand-alone FLUKA model of the IR7 region, incorporating magnetic fields generated based on the underlying optics. As source distribution, the second step uses the impact distribution of particles on the crystal and collimators derived in the first step. The geometry of each collimator or magnet is accurately represented, enabling also successive thermo-mechanical simulations with other codes (see, for example, Ref. [23]) or the assessment of the quench margin, as presented in this paper.

POWER DEPOSITION ESTIMATES FOR RUN 3

In this section, we present FLUKA power deposition calculations for cold magnets downstream of the betatron cleaning insertion, considering Run 3 beam parameters (6.8 ZTeV). The results are compared to a previous study for the LHC design case with 7 ZTeV reported in Ref. [5], which assumed a different beam optics and a different bending angle for the crystals. The collimation system settings

ISBN: 978-3-95450-253-0 ISSN: 2673-5571 doi:10.18429/JACoW-HB2023-WEC2C1

Table 1: Collimator half-gaps in IR7 assumed in the FLUKA studies, expressed as the number of beam σ for a normalized transverse beam emittance of 3.5 µm rad. The secondary collimator settings correspond to secondary collimators downstream of the crystal.

Collimator	Settings [σ]
Primary collimators (TCP)	5
Crystal (TCPC)	4.75
Secondary collimators (TCSG)	6.5
Shower absorbers (TCLA)	10

in terms of beam sigma were the same in both studies, as detailed in Table 1. The power deposition density in the coils is evaluated via a 3D cylindrical mesh, featuring longitudinal bins of approximately 10 cm and azimuthal bins of 2°. Assuming steady-state losses (t >5 s) and continuous cooling provided by the helium, the power deposition density has to be averaged over the radial thickness of the inner coils in order to account for the heat transfer during the loss period. In the following, we always report the maximum azimuthal value for the power density, which usually occurs on the horizontal plane. All results are normalized to a power loss of 30 kW, which corresponds to a particle loss rate of 3.36×10^8 $^{208}Pb^{82+}$ ions/s.

The longitudinal peak power density distributions within the superconducting magnets are shown in Fig. 4 (top plot). The results for both the clockwise (Beam 1) and anticlockwise (Beam 2) circulating beams are compared. It can be observed that for Beam 2 at 6.8 ZTeV (2023 optics), the highest power density in the dipoles (MB.A9) reaches approximately 8 mW/cm^3, while for Beam 1 at 7 ZTeV (previous optics) this value was about 12 mW/cm^3. Both values are lower than the approximate quench level of 15 mW/cm^3, which is based on the assumption that the quench margin at 6.8 ZTeV to 7 ZTeV is a few ten percent lower than the 20 mW/cm^3 quench level observed during a quench test at 6.37 ZTeV in 2015 [24]. Compared to the previous studies, a different peak power density distribution is observed in half-cells 11/12 and 13, which can be mainly attributed to the different beam optics. In the new studies, based on the 2023 configuration, the maximum power density occurs in the MQ.11 quadrupole. For quadrupoles, the quench level is, however, higher than dipoles and is estimated to be two times above the 20 mW/cm^3 observed in the simulations [25].

The bottom plot of Fig. 4 compares the energy loss distribution on the cold aperture derived in this study (Beam 2, 2023 optics, 6.8 ZTeV) with the one obtained in Ref. [5] (Beam 1, previous optics, 7 ZTeV). In both cases, the bending angle of the crystal is similar. However, due to the optics being different, one can observe a different distribution of fragment losses, reflecting the findings from the power deposition studies. This is particularly visible for $^{206}Pb^{82+}$, impacting quadrupole MQ.13 instead of MQ.11, and $^{201}Tl^{81+}$, hitting MB.A11 instead of MB.B9.

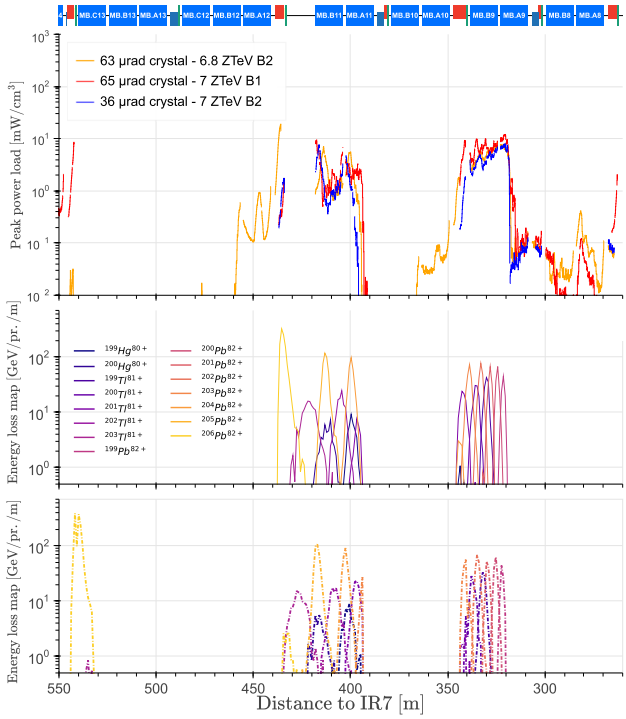

Figure 4: Top: simulated longitudinal distribution of the peak power density in the inner coils of DS magnets (30 kW power loss). The beam direction is from right to left. The 7 ZTeV results are from Ref. [5]. Middle: Energy loss map on the cold magnet aperture in DS and arc for Beam 2 (2023 configuration, 6.8 ZTeV ion beams); Bottom: energy loss map for Beam 1 [5] (previous optics, 7 ZTeV ion beams). Both loss maps show the most abundant heavy fragments lost in this region.

CONCLUSIONS

The LHC crystal-assisted collimation system plays an essential role for heavy ion operation during Run 3 and beyond. This study utilized FLUKA to estimate the power density deposited in the superconducting coils of DS magnets downstream of the betatron cleaning region. In particular, we presented studies for the 2023 heavy-ion run, which marked the start of the high-luminosity LHC era for the heavy-ion program. Although there is some remaining uncertainty regarding quench levels at 6.8 ZTeV and 7 ZTeV, this work confirms the prospects of using crystals as primary collimators. With particle loss rates equivalent to beam power losses of 30 kW, the simulation suggests that the power density remains below the quench level of dipoles and quadrupoles. Assuming nominal HL-LHC heavy ion parameters, this power loss corresponds to a beam lifetime of about 0.2 h. The present studies did not take into account machine imperfections, which can still affect the actual heat deposition in the magnets. Future studies are foreseen to perform benchmarks against beam loss monitor measurements from the 2023 run at 6.8 ZTeV, which will be presented in a future publication.

ISBN: 978-3-95450-253-0 ISSN: 2673-5571 doi:10.18429/JACoW-HB2023-WEC2C1

REFERENCES

[1] R. Bruce, M. A. Jebramcik, J. M. Jowett, T. Mertens, and M. Schaumann, "Performance and luminosity models for heavy-ion operation at the CERN Large Hadron Collider," *Eur. Phys. J. Plus*, vol. 136, no. 7, 2021. doi:10.1140/epjp/s13360-021-01685-5

[2] J. Coupard *et al.*, "LHC Injectors Upgrade," CERN, Geneva, Switzerland, Tech. Rep. CERN-ACC-2016-0041, 2016. doi:10.17181/CERN.L6VM.UOMS

[3] O. S. Brüning *et al.*, "LHC Design Report," CERN, Geneva, Switzerland, Tech. Rep. CERN-2004-003-V-1, 2004. doi:10.5170/CERN-2004-003-V-1

[4] P. D. Hermes *et al.*, "LHC Heavy-Ion Collimation Quench Test at 6.37 Z TeV," CERN, Geneva, Switzerland, Tech. Rep. CERN-ACC-NOTE-2016-0031, 2016. https://cds.cern.ch/record/2136828

[5] J. Potoine *et al.*, "Power deposition studies for standard and crystal-assisted heavy ion collimation in the CERN Large Hadron Collider," *Phys. Rev. Accel. Beams*, vol. 26, no. 9, p. 093 001, 2023. doi:10.1103/PhysRevAccelBeams.26.093001

[6] S. Redaelli, R. Bruce, A. Lechner, and A. Mereghetti, "High-Luminosity Large Hadron Collider (HL-LHC), Chapter 5: Collimation system," Tech. Rep. CERN-2020-010, 2020, pp. 87–114. doi:10.23731/CYRM-2020-0010.87

[7] E. B. Holzer *et al.*, "Beam loss monitoring system for the LHC," in *Proc. IEEE Nuclear Science Symposium*, Puerto Rico, USA, Oct. 2005, pp. 1052–1056. doi:10.1109/NSSMIC.2005.1596433

[8] V. M. Biryukov, Y. A. Chesnokov, and V. I. Kotov, *Crystal Channeling and Its Application at High-Energy Accelerators*. Springer, Berlin, Germany, 1997. doi:10.1007/978-3-662-03407-1

[9] W. Scandale and A. Taratin, "Channeling and volume reflection of high-energy charged particles in short bent crystals. crystal assisted collimation of the accelerator beam halo," *Phys. Rep.*, vol. 815, pp. 1–107, 2019. doi:10.1016/j.physrep.2019.04.003

[10] R. Bruce *et al.*, "HL-LHC operational scenarios for Pb-Pb and p-Pb operation," CERN, Geneva, Switzerland, Tech. Rep. CERN-ACC-2020-0011, 2020. https://cds.cern.ch/record/2722753

[11] M. D'Andrea *et al.*, "Crystal Collimation of 20 MJ Heavy-Ion Beams at the HL-LHC," in *Proc. IPAC'21*, Campinas, Brazil, May 2021, pp. 2644–2647. doi:10.18429/JACoW-IPAC2021-WEPAB023

[12] *FLUKA website*, https://fluka.cern/.

[13] G. Battistoni *et al.*, "Overview of the FLUKA code," *Ann. Nucl. Energy*, vol. 82, pp. 10–18, 2015. doi:10.1016/j.anucene.2014.11.007

[14] C. Ahdida *et al.*, "New Capabilities of the FLUKA Multi-Purpose Code," *Front. Phys.*, vol. 9, p. 788 253, 2022. doi:10.3389/fphy.2021.788253

[15] D. Mirarchi, G. Hall, S. Redaelli, and W. Scandale, "A crystal routine for collimation studies in circular proton accelerators," *Nucl. Instrum. Methods Phys. Res., Sect. B*, vol. 355, pp. 378–382, 2015. doi:10.1016/j.nimb.2015.03.026

[16] F. Forcher, "An improved simulation routine for modelling coherent high-energy proton interactions with bent crystals," Bachelor thesis, Padua University, Italy, 2017. https://cds.cern.ch/record/2314775

[17] P. Schoofs, F. Cerutti, A. Ferrari, and G. Smirnov, "Benchmark of the FLUKA model of crystal channeling against the UA9-H8 experiment," *Nucl. Instrum. Methods Phys. Res., Sect. B*, vol. 355, pp. 374–377, 2015. doi:10.1016/j.nimb.2015.03.074

[18] A. Mereghetti *et al.*, "SixTrack-Fluka Active Coupling for the Upgrade of the SPS Scrapers," in *Proc. IPAC'13*, Shanghai, China, May 2013, pp. 2657–2659. https://jacow.org/IPAC2013/papers/WEPEA064.pdf

[19] *SixTrack website*, http://sixtrack.web.cern.ch/SixTrack/.

[20] R. D. Maria *et al.*, "SixTrack Version 5: Status and New Developments," in *Proc. IPAC'19*, Melbourne, Australia, May 2019, pp. 3200–3203. doi:10.18429/JACoW-IPAC2019-WEPTS043

[21] E. Skordis *et al.*, "FLUKA coupling to Sixtrack," in *CERN Yellow Rep. Conf. Proc.*, vol. 2, CERN, Geneva, Switzerland, 2020, pp. 17–25. doi:10.23732/CYRCP-2018-002.17

[22] R. Cai *et al.*, "Simulation of Heavy-Ion Beam Losses with Crystal Collimation," in *Proc. IPAC'22*, Bangkok, Thailand, 2022, pp. 2082–2086. doi:10.18429/JACoW-IPAC2022-WEPOTK018

[23] M. Cauchi *et al.*, "Thermomechanical response of Large Hadron Collider collimators to proton and ion beam impacts," *Phys. Rev. Spec. Top. Accel. Beams*, vol. 18, no. 4, p. 041 002, 2015. doi:10.1103/PhysRevSTAB.18.041002

[24] M. Schaumann, J. Jowett, C. B. Castro, R. Bruce, A. Lechner, and T. Mertens, "Bound-free pair production from nuclear collisions and the steady-state quench limit of the main dipole magnets of the CERN Large Hadron Collider," *Phys. Rev. Accel. Beams*, vol. 23, no. 12, p. 121 003, 2020. doi:10.1103/PhysRevAccelBeams.23.121003

[25] B. Auchmann *et al.*, "Testing beam-induced quench levels of LHC superconducting magnets," *Phys. Rev. Spec. Top. Accel. Beams*, vol. 18, no. 6, p. 061 002, 2015. doi:10.1103/PhysRevSTAB.18.061002